

Oxygen-vacancy donor-electron center in $Y_3Al_5O_{12}$ garnet crystals: Electron paramagnetic resonance and dielectric spectroscopy study

V. Laguta¹, M. Buryi¹, P. Arhipov², O. Sidletskiy², O. Laguta³, M. G. Brik^{4,5,6} and M. Nikl¹

¹*Institute of Physics Academy of Science of Czech Republic, Cukrovarnická 10, 162 00 Prague 6, Czech Republic*

²*Institute for Scintillation Materials, National Academy of Sciences of Ukraine, Nauky Avenue 60, 61072 Kharkiv, Ukraine*

³*Brno University of Technology, Central European Institute of Technology, Purkyňova 656/123, 612 00 Brno, Czech Republic*

⁴*CQUPT-BUL Innovation Institute & College of Sciences, Chongqing University of Posts and Telecommunications, Chongqing 400065, People's Republic of China*

⁵*Institute of Physics, University of Tartu, W. Oswaldi 1, Tartu 50411, Estonia*

⁶*Institute of Physics, Jan Długosz University, Armii Krajowej 13/15, PL-42200 Częstochowa, Poland*



(Received 24 October 2019; revised manuscript received 27 December 2019; published 15 January 2020)

The F^+ center consisting of an electron trapped at an oxygen vacancy (V_O) was investigated in oxygen deficient $Y_3Al_5O_{12}$ (YAG) garnet crystals by electron paramagnetic resonance (EPR) techniques. The measurements were performed in the wide temperature interval 5–450 K and the frequency range 9.4–350 GHz using both the conventional continuous-wave and pulse EPR experiments. Pulse electron-nuclear double resonance was applied to resolve the hyperfine interaction of the trapped electron with surrounding nuclei. The measurements show that at low temperatures, $T < 50$ K, the EPR spectrum of the F^+ center is anisotropic with g factors in the range 1.999–1.988 and originates from three magnetically inequivalent positions of the center in a garnet lattice. As the temperature increases, the EPR spectrum becomes isotropic suggesting a motional averaging of the anisotropy due to motion of the F^+ -center electron between neighboring oxygen vacancies. With further increase of temperature up to $T > 200$ K, we observed delocalization of the F^+ -center electron into the conduction band with the activation energy about 0.4–0.5 eV that resulted in substantial narrowing of the EPR spectral line with simultaneous change of its shape from Gaussian to Lorentzian due to disappearance of the Fermi contact hyperfine field at ^{27}Al and ^{89}Y nuclei. Such temperature behavior of the F^+ -center electron in YAG is completely similar to behavior of a donor electron in a semiconductor. Our findings are further supported by measurements of the conductivity and dielectric properties. In particular, these data show that the electrons in the conduction band are not homogeneously distributed in the crystal: There are highly conductive regions separated by poorly conductive dielectric layers. This leads to the so-called Maxwell-Wagner dielectric relaxation with huge apparent dielectric constant at low frequencies. This paper reports an observation of a donorlike behavior of an F^+ center in wide band-gap insulating crystals.

DOI: [10.1103/PhysRevB.101.024106](https://doi.org/10.1103/PhysRevB.101.024106)

I. INTRODUCTION

$Y_3Al_5O_{12}$ (YAG) and isomorphic $Lu_3Al_5O_{12}$ (LuAG) crystals as well as their ceramics and powders doped with rare-earth ions are widely exploited as laser media [1–4]; luminescent and scintillation materials in high-tech industry, medicine, security imaging, and monitoring systems [5–7]; in solid-state white light sources [8], etc. In spite of their favorable properties, the main demerit of both YAG and LuAG is the presence of slow components in the scintillation decay and afterglow, which cause serious degradation of the efficiency, light yield, and timing characteristics [9,10]. It is commonly accepted that these slower decay components are related to the host defects, which temporarily trap charge carriers before their radiative recombination at the emission centers. The garnet's luminescence efficiency is also influenced by various host defects. Among them, the so-called antisite ion defects; i.e., Y or Lu at the octahedral Al site and oxygen vacancies are the most frequently met intrinsic defects in garnet crystals [11–13]. Moreover, both these defects can be coupled into pairs as was demonstrated in $YAlO_3$ [14]. The oxygen vacancy

(V_O) naturally serves as an effective trap for electrons. It can be thus filled by one or two electrons forming the charged F^+ and neutral F° centers, respectively. In spite of the fact that the F -type centers usually produce prominent absorption bands in the visible or UV region, unambiguous identification of these centers by optical methods only is quite questionable, especially in noncubic complex oxides, where the actual local structure of the considered center can hardly be determined. In this respect, the F^+ centers, being paramagnetic, can be successfully identified and studied at the atomistic level by electron paramagnetic resonance (EPR) as was demonstrated for many oxide materials [6,15–18].

Probably the first ever indication of the EPR detection of an electron trapped at V_O in YAG was published by Mori [19]. A single EPR line at the g factor 1.995 ± 0.002 was observed in the additively colored crystal. This EPR line correlated with the appearance of three broad absorption bands peaked at 1.2×10^4 , 2.0×10^4 , and 2.8×10^4 cm^{-1} . It was assumed that the observed EPR line as well as the absorption bands originate from an unpaired electron trapped

at an oxygen vacancy (F^+ center). However, no further studies were performed with this EPR signal as it was uninformative to make a valid conclusion about the origin, local structure, and thermal stability of the corresponding center. Later, a similar spectrum (an isotropic line at g factor 1.996) was revealed in YAG crystals either γ irradiated or photoirradiated by an UV nitrogen laser at 77 K [20]. In the crystals reduced at 1500–1650 K a single EPR line at $g = 1.994$ with the small anisotropy, $\Delta g = 0.0002$ was also measured [21]. Again, except for this EPR signal observation and possible identification of its F^+ -center origin, no further analysis of this spectrum was made. A strong EPR signal with $g = 1.994$ was observed in a YAG crystal doped by Si [22]. This crystal was slightly blue colored. The spectrum in this crystal was attributed to an electron trapped at V_O nearby a Si ion, i.e., a F^+ -Si complex. This center was stable at room temperature and existed without any prior irradiation. Note that a weak spectral line with g factor 1.994 was also observed in highly pure transparent YAG and LuAG crystals, but it was difficult to interpret its origin as it appeared only after X-ray irradiation at liquid nitrogen temperature together with the spectrum coming from trapped hole centers, and these two spectra are strongly overlapped [23].

There is also an uncertainty in the temperature stability of such an oxygen-vacancy-based center in YAG and, respectively, in the interpretation of corresponding thermally stimulated luminescence peaks and absorption and luminescence bands (see, e.g., [20,24,25], and a review paper [6]) which appear in crystals after x-ray and UV irradiation at 77 and 300 K. Some of the mentioned peaks may also arise from the antisite defect-based traps created by Y cations occupying the octahedral Al sites and vice versa. They serve as effective traps for electrons as well. Moreover, the Y antisite ion can be coupled with oxygen vacancy creating the $Y_{Al}^{3+} - V_O$ defect acting as an electron trap. Such defects were identified by EPR in $YAlO_3$, for instance [14]. However, the EPR spectra of similar defects were never observed in YAG or LuAG, despite clear indications of their possible existence in garnets from the luminescence and thermally stimulated luminescence (TSL) data [10,24,26,27].

In this paper we present the results of detailed EPR investigation of the blue-colored YAG crystals which surely contain a high concentration of oxygen vacancies. For comparison, an annealed-in-air YAG crystal was measured as well. To overcome saturation effects in the EPR spectra due to extremely long spin-lattice relaxation time of the oxygen-vacancy center and to resolve anisotropy of the g factor, a major part of the measurements at low temperatures was performed at the Q microwave band at 34 GHz using the spin-echo detected EPR [28]. Moreover, some measurements were performed at frequencies up to 350 GHz. To resolve the hyperfine interaction of the trapped electron at oxygen vacancy with its surroundings, the pulse electron-nuclear double resonance (ENDOR) technique was applied in the Q microwave band. A model of the F^+ center in YAG is proposed on the basis of the obtained experimental data. The model assumes localization of an electron within oxygen-vacancy space at $T < 50$ K, as in MgO , and its further behavior with temperature increase is similar to that of the donor electron in a semiconducting material.

II. EXPERIMENTS

The crystals were grown by the Czochralski method under Ar+CO reducing atmosphere at $\approx 1700^\circ\text{C}$. Details of the crystal growth are presented in [29]. Because of the growth under reducing conditions the as-grown YAG possesses a high concentration of color centers linked to electron capture by oxygen vacancies. The coloration even deepens under illumination with daylight. However, these crystals become completely transparent after annealing in air atmosphere at 900°C – 1000°C . Their optical properties under different thermal annealing are studied in [30]. For measurements, the crystals were cut in the (100) planes in a typical shape of about $2 \times 2.2 \times 4 \text{ mm}^3$ and $1 \times 1.1 \times 1.3 \text{ mm}^3$.

The EPR measurements were performed using a Bruker E580 spectrometer operated at the X (9.4 GHz) and Q (34 GHz) microwave (MW) bands in both conventional continuous-wave (cw) and pulse modes at the temperatures from 450 K down to 5 K. In addition, to resolve hyperfine interaction in the EPR signals, the pulse electron-nuclear double resonance technique was utilized as well. The ENDOR spectra were measured at the Q MW band using the Mims [31] and Davies pulse sequences [32].

Additional EPR measurements were performed with the homemade high-frequency spectrometer operated at frequencies from 82.5 up to 1100 GHz in the magnetic field 0–15 T at the temperature 4.6 and 260 K. The field sweep resolution was 28 000 points for the 0–15 T range with the sweep time of 100–150 min for one spectrum. Details of this spectrometer design can be found in [33] and in supplementary material to that publication.

III. EXPERIMENTAL RESULTS

A. Cw EPR data

The EPR spectra measured at 175 K in the colored (a) and transparent (b) crystals are shown in Fig. 1, as an example. The colored sample showed a strong signal at $B \approx 337$ mT, g factor 1.994, and several weaker signals attributed to the well-known Fe^{3+} spectrum in YAG crystals [34]. As an accidental impurity, these ions are always present in YAG or LuAG crystals at a concentration of 5–50 ppm. Fe^{3+} usually penetrates into the crystal from Al_2O_3 oxide used in crystal growth. It is shown below that the strong spectral line at 337 mT ($g = 1.994$) originates from an electron trapped at oxygen vacancy, usually called the F^+ center [15]. The F^+ signal completely disappears after annealing of the colored crystal in air at 900°C for about 6 h [spectrum (b) in Fig. 1] when the crystal becomes completely transparent thus confirming that this signal is indeed related to the oxygen vacancies removed by annealing. Note that the Fe^{3+} concentration also decreases with this annealing due to recharge of the iron ions [21]. A similar spectrum at a g factor of about 1.994 was measured by us in YAG doped by Si [22], in the x-ray irradiated YAG and LuAG crystals doped by Sc and Mg [6], and by Mori in a YAG crystal colored by annealing in Al atmosphere [19]. In transparent crystals and crystals doped with Mg, the F^+ spectrum appears only after x-ray irradiation of the crystals at 77 K together with a much stronger spectrum from the O^- hole center [Fig. 1, spectrum (c)].

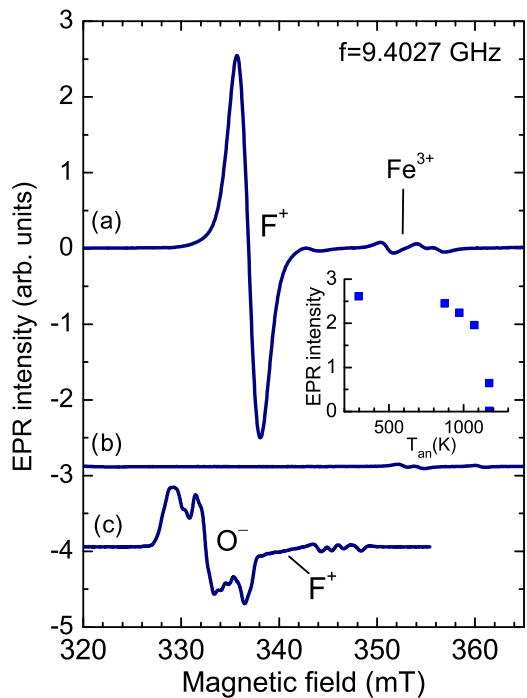


FIG. 1. X-band EPR spectrum in YAG crystals taken at 175 K before (a) and after (b) annealing in air atmosphere at 900 °C for 6 h. Strong signal at ≈ 337 mT is produced by the F^+ center; other weak intensity signals are due to the Fe^{3+} impurity ions. (c) For comparison, x-ray induced EPR spectrum measured at 25 K in YAG doped by 500 ppm Mg is shown as well. The F^+ signal appears as a shoulder at the right side of the strong O^- hole spectrum (for details, see [23]). For all spectra, the magnetic field was oriented along the [100] cubic axis. The inset shows the dependence of the F^+ spectral intensity on pulsed annealing temperature for the annealing time of 1 h.

The F^+ center in YAG has several characteristic features. For instance, in contrast to a similar oxygen-vacancy center in $YAIO_3$ [14], the F^+ spectrum in YAG can be measured even at room temperature and without any prior irradiation. Its spectral line is completely isotropic at these temperatures and the g factor only slightly deviates from the free-electron g factor ($g-g_s = 0.0083$). In the present paper, we consider this center in detail.

An undistorted F^+ spectrum could be measured by the cw EPR technique down to about 50 K. At lower temperatures, due to long spin-lattice relaxation time, the intensity of the spectral features is decreased and their shape becomes distorted. To obtain the true undistorted spectrum at $T < 50$ K the spin-echo detected field-sweep method (EDEPR) [28] was employed. Another fact to which we pay attention is that the spectral linewidth decreases with temperature increase. This is an unusual feature which indicates a fast motion of electrons between inequivalent defect positions in the lattice. When this motion becomes slow at low temperature, the spectral line becomes asymmetric or even splits into several components according to the number of magnetoinequivalent positions of a center [35,36].

In order to confirm whether the spectrum is anisotropic at low temperatures, its temperature dependence was measured in the Q band, where due to four-times larger frequency

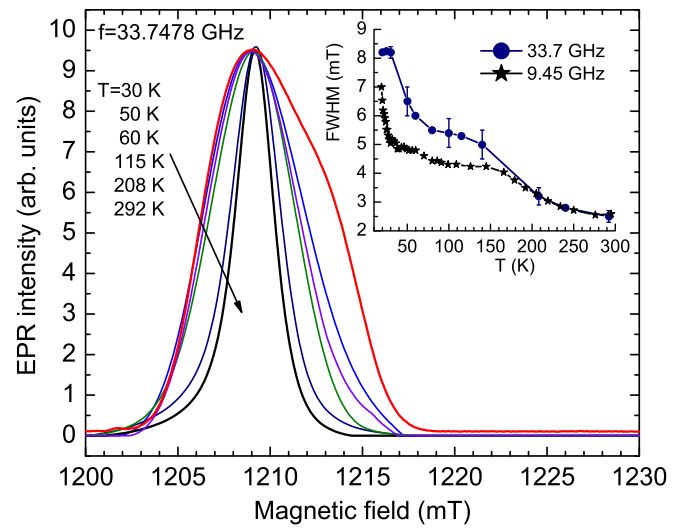


FIG. 2. Q -band EPR absorption spectra in YAG crystal at different temperatures normalized in intensity to the spectrum at 292 K and $B \parallel [100]$. The spectrum at 30 K (red line) was obtained by the spin-echo detected field-sweep method. Other spectra were measured by a conventional cw EPR technique with integration of the original EPR signals. The inset shows temperature dependence of the FWHM linewidth of the spectral lines measured at 9.45 and 33.7 GHz.

the separation between components in the spectrum should increase as well. Figure 2 presents such spectra taken at a few temperatures to demonstrate temperature behavior of the F^+ spectrum.

The temperature dependence of the full width at half maximum (FWHM) of the spectral line measured at two MW frequencies is presented in the inset to Fig. 2. In particular, one can see that the spectrum width substantially increases with temperature decrease and finally at $T < \sim 40$ K its shape becomes remarkably asymmetric. This asymmetric line can be fitted by three Gaussians (Fig. 3). The difference in

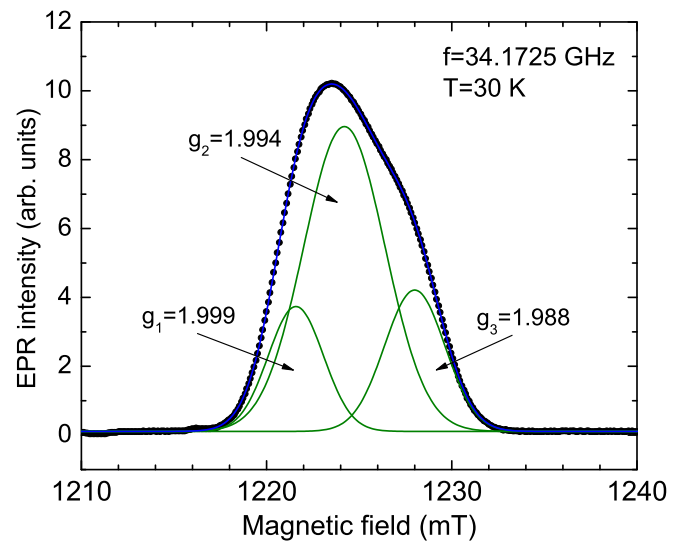


FIG. 3. Decomposition of the EDEPR line into three Gaussian components demonstrating anisotropy of the g factor of the F^+ center at low temperatures, $T < \sim 40$ K.

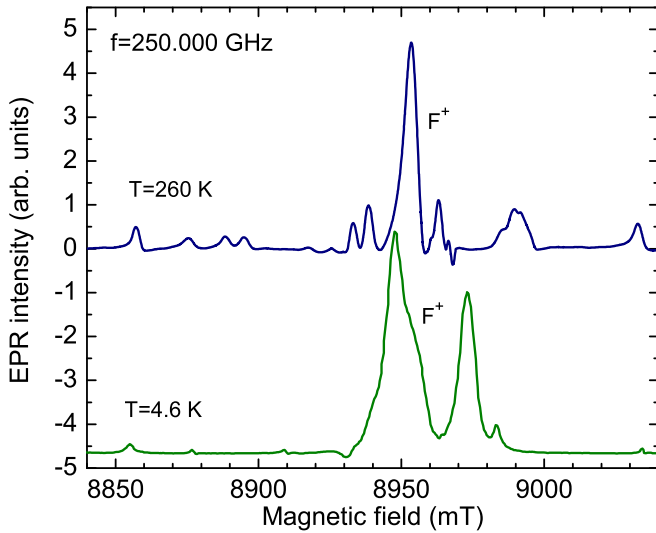


FIG. 4. EPR spectrum of the F^+ center in colored YAG crystal measured at the frequency 250 GHz at 260 K (upper spectrum, fast motion regime) and 4.6 K (bottom spectrum, slow motion regime). Other low-intensity lines belong to Fe^{3+} resonances. The crystal has arbitrary orientation with respect to magnetic field.

the g factors of the two outermost lines, $g_3 - g_1 = 0.011$, approximately characterizes anisotropy of the g factor, which is small as compared to the F^+ center in YAP, for example [14], where the g factor anisotropy is $g_3 - g_1 = 0.17$. Obviously, the three-component spectrum originates from three magnetically inequivalent positions of the considered center in the YAG lattice. There are 96 positions of the oxygen vacancy in the YAG unit cell which, however, transform one into another by symmetry operations of the $Ia3d(O_h^{10})$ space group of the YAG lattice [37]. These magnetically inequivalent positions of the F^+ center correspond to three different directions of the Al(IV)– V_O –Al(VI) chains (paths) in the unit cell, where each of the V_O sites possesses symmetry C_1 . The anisotropy of the F^+ center in YAG is determined by involving the Al and Y p and d orbitals in the predominantly s -type ground state of the F^+ center. This is further supported by the data of ENDOR measurements. However, exact determination of the g tensor components and its principal axes directions was not possible due to weak splitting in the spectrum.

B. High-frequency EPR measurements

The F^+ center was further studied by EPR measurements at high frequencies from 90 up to 350 GHz. Even at these frequencies there is only one spectral line from the F^+ center at room temperature, which only slightly increases in width as the frequency increases, but does not split. For instance, the FWHM linewidth is only 3.5–4.0 mT at the frequency 250 GHz (Fig. 4, upper spectrum), while the expected splitting for the static spectrum (slow motion regime) due to g factor anisotropy, depending on crystal orientation, should be up to 45 mT at this frequency. Therefore, even at this high frequency the spectrum is still motionally averaged at room temperature (fast motion regime). On the contrary, the spectrum becomes clearly split into a few components at low temperature (Fig. 4,

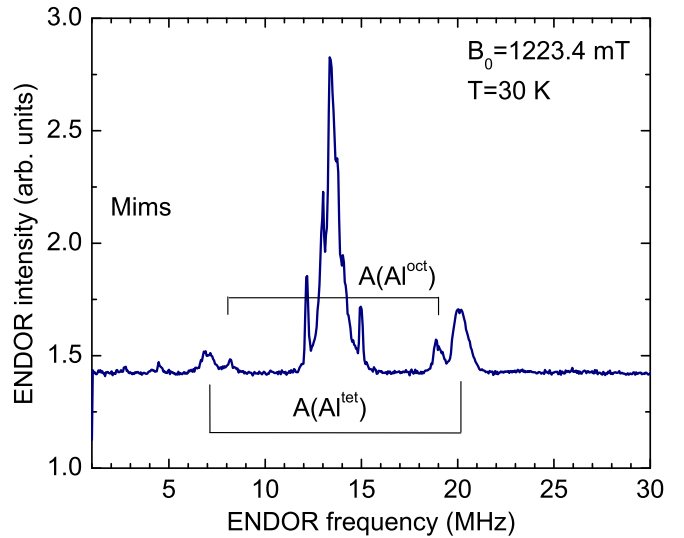


FIG. 5. ENDOR spectrum for the F^+ center measured by the Mims pulse sequences and $B \parallel [111]$.

bottom spectrum). Note that at these high MW frequencies, the F^+ spectral line is superimposed on the Fe^{3+} central transition spectrum that essentially complicates separation of the F^+ resonances at most crystal orientations. This difficulty even increases with increase of the MW frequency due to shifting of the Fe^{3+} central transition lines to the range of g factor values for the F^+ center at all crystal orientations as g factors of both centers practically coincide.

C. ENDOR data

A characteristic feature of any F^+ center is delocalization of electron density over surrounding cations that leads to Fermi contact hyperfine (HF) interaction of the electron spin with nuclear magnetic moments. The corresponding HF splitting was not resolved in the EPR spectrum due to its small value. Therefore, the HF interaction was measured by the ENDOR technique. The ENDOR spectrum measured by the Mims pulse sequence [31] (the Davies pulse sequence gives the same spectrum, but of lower intensity) is shown in Fig. 5.

The spectrum contains a group of strong lines centered near the Larmor frequency, 13.63 MHz, of the ^{27}Al isotope, which has the nuclear spin $I = 5/2$ and natural abundance 100%. The splitting between the outermost lines in the group is about 3 MHz. Other well-visible lines grouped into two duplets are separated by much larger frequency distances, 13.2 and 10.7 MHz [$A(\text{Al}^{\text{oct}})$ and $A(\text{Al}^{\text{tet}})$ in Fig. 5]. The positions of these two duplets do not depend markedly on the crystal orientation, while the lines near the ^{27}Al Larmor frequency are substantially changed in both intensity and frequency positions being, however, within the 3.6 MHz frequency interval. This suggests that this group of lines originates from ^{27}Al nuclei distant to the paramagnetic center and that the complex ENDOR structure around the ^{27}Al Larmor frequency originates mainly from quadrupole transitions of the ^{27}Al nuclei.

The observed ENDOR spectrum can be interpreted using the following spin Hamiltonian:

$$\mathbf{H} = \beta \mathbf{B} g \mathbf{S} - g_n \beta_n \mathbf{B} \mathbf{I} + \sum_i \left\{ S A_i I_i + \frac{\nu_Q}{2} \left[3I_{iz}^2 - I_i(I_i + 1) + \frac{1}{2} \eta (I_{i+}^2 - I_{i-}^2) \right] \right\}, \quad (1)$$

where $\nu_Q = \frac{3e^2qQ}{h2I(2I-1)}$ is the quadrupole frequency and eQ is the quadrupole moment of a nucleus. The x , y , z axes are the principal axes of the electric field gradient (EFG) tensor \mathbf{V} , where $|V_{zz}| \geq |V_{xx}| \geq |V_{yy}|$, $eQ = V_{zz}$, $\eta = \frac{V_{xx} - V_{yy}}{V_{zz}}$. The first two terms in the spin Hamiltonian (1) describe the electron and nuclear Zeeman interactions, the third term is the electron-nuclear HF interaction, and the last term corresponds to the quadrupole interaction of the nuclear spins I_i with the electric field gradient.

Because for distant ^{27}Al nuclei the HF interaction is negligibly small as compared to the quadrupole one, the HF term in the spin Hamiltonian (1) can be omitted and the ENDOR resonances will thus depend exclusively on the EFG value. For the tetragonal symmetry of the EFG tensor and the condition $g_n \beta_n B I \gg \nu_Q$ that is valid for both the tetrahedral and octahedral Al sites in the field of 1.2 T, the solution of the spin Hamiltonian (1) neglecting the second-order effects is simple:

$$\nu_m = \nu_L - \nu_Q(m - 1/2) \frac{3\cos^2\theta - 1}{2}. \quad (2)$$

Here $\nu_L = \beta_n g_n B$ and θ is the angle between \mathbf{B} and the direction of the z axis of the EFG tensor. This axis in YAG coincides with the direction of the tetrahedron and octahedron distortions, (100) and (111) crystal axes, respectively. Taking $\theta = 0$ that corresponds to maximum splitting between quadrupole transitions, we found that the splitting between the $5/2 \leftrightarrow 3/2$ and $-5/2 \leftrightarrow -3/2$ transitions will be $4\nu_Q$. The quadrupole frequency ν_Q for ^{27}Al is known from NMR measurements [38,39]. It is 0.915 and 0.0955 MHz for the tetrahedral and octahedral Al sites, respectively. This agrees well with the positions of the quadrupole satellites measured by ENDOR taking into account that the actual orientation of the [100] crystal axis is not exactly along the magnetic field; i.e., the angle θ in Eq. (2) is only close to zero. In particular, due to ten times larger quadrupole frequency for the tetrahedral Al sites, only the quadrupole transitions from these Al nuclei are resolved in the ENDOR spectrum. Besides, the spectrum contains a broad background line, which originates from the contribution of Al nuclei located at middle distances from the oxygen vacancy. For these nuclei, EFG is distributed in both the value and direction of the principal axes that leads to essential broadening of the quadrupole transitions. Moreover, the HF interaction cannot be neglected for these nuclei as well. It will also differ in value depending on the location of those nuclei. Only nuclei situated far enough from the oxygen vacancy produce sharp narrow spectral lines from quadrupole transitions.

The HF term in the spin Hamiltonian (1) cannot be neglected for the Al nuclei neighboring the oxygen vacancy. Moreover, it seems that the EFG at Al nuclei in the nearest

position at the oxygen vacancy is so large that only the $1/2 \leftrightarrow -1/2$ central transition is seen in the ENDOR spectrum. For the central transition in the first-order approximation the resonance frequencies are determined by the following expression [40]:

$$\nu_{1/2} = |\nu_L \pm A_i/2|. \quad (3)$$

Here we also assumed an isotropic HF interaction in accordance with our experiment (two doublets in Fig. 5 practically do not depend on crystal orientation). Using Eq. (3) and the data in Fig. 5, the following HF constants were determined for two Al nuclei: $A_1 = 10.7$ MHz and $A_2 = 13.2$ MHz. Obviously, the larger HF constant describes interaction of the trapped electron in the F^+ center with the Al nucleus arranged in the tetrahedral coordination due to shorter O – Al^{tet} distance (0.1761 nm in the regular lattice [37]) as compared to the O – Al^{oct} distance (0.1937 nm in the regular lattice). This assignment of the ENDOR peaks is further supported by the fact that the number of Al tetrahedral positions is 1.5 times larger than that for the octahedral Al. However, the main reason for the remarkably different intensities of the two doublets is related to relaxation times, which should be different at these two Al sites, as even in the regular YAG lattice EFG at the tetrahedral site is ten times larger than at the octahedral one. That is, the quadrupole interaction effectively shortens relaxation time which, in turn, influences the ENDOR intensity.

An electron trapped at the oxygen vacancy must also interact with ^{89}Y nuclei which have the nuclear spin $1/2$, the natural abundance is 100% but the Larmor frequency is very small, 2.57 MHz even in the 1.2 T field. These nuclei may be responsible for two weak lines at 2.7 and 4.5 MHz. However, this assignment is not convincing as most probably the ^{89}Y Larmor frequency and the HF constant values are comparable. As a result, ^{89}Y resonances could not be visible due to the limitation in ENDOR frequencies to 1 MHz. The measurements in much stronger magnetic fields can clarify the situation with the ^{89}Y ENDOR. On the other hand, Al ions play the major role in the interaction of a trapped electron with its surroundings that is reflected in large HF constants for Al nuclei.

D. Model of the F^+ center in YAG and behavior of the trapped electron with temperature

The above presented data clearly suggest that the EPR signal with the nearly isotropic g factor in the 1.999–1.988 range in YAG crystals belongs to an electron trapped at an oxygen vacancy (Fig. 6). Since the HF interaction of the trapped electron with surrounding nuclei is predominantly isotropic, Fermi contact type, the wave function of the trapped electron is nearly spherically symmetrical, like s -type orbitals. This corresponds to the classical F^+ center (similar to the F^+ center in MgO [15] or Al_2O_3 [41]), when the trapped electron is mainly located within the vacancy space, but its wave function has nonzero density at surrounding cations [15]. The delocalization of electron density leads to a partial contribution of the Y $4d$ and Al $3p$ orbitals into the F^+ -center ground state that explains the small negative shift of its g factor.

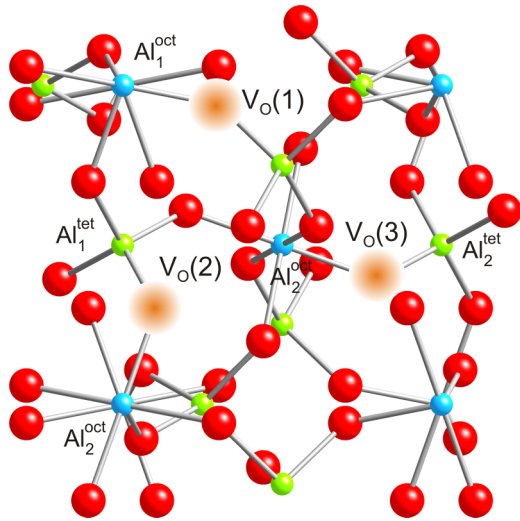


FIG. 6. Fragment of the YAG crystal structure (projection into (001) plane) with an oxygen-vacancy center at three magnetically inequivalent positions.

The most interesting feature of the oxygen-vacancy center in YAG is the essential narrowing of its spectral line with temperature increase, which suggests possible motion in the center. Let us discuss this phenomenon, at least qualitatively. Figure 7 shows the temperature dependence of the peak-to-peak linewidth (distance between two peaks of the first derivative of spectral line) measured from 10 up to 450 K at 9.4 GHz. This simply measurable parameter of the spectral line is commonly used for characterization of lines with different shapes, especially when the shape of a line changes with temperature. In our case, the spectral line is complex at $T < 50$ K (Fig. 3). It becomes a single Gaussian between 50 and 180 K, and changes from Gaussian to Lorentzian at 150–350 K [Fig. 7(b)].

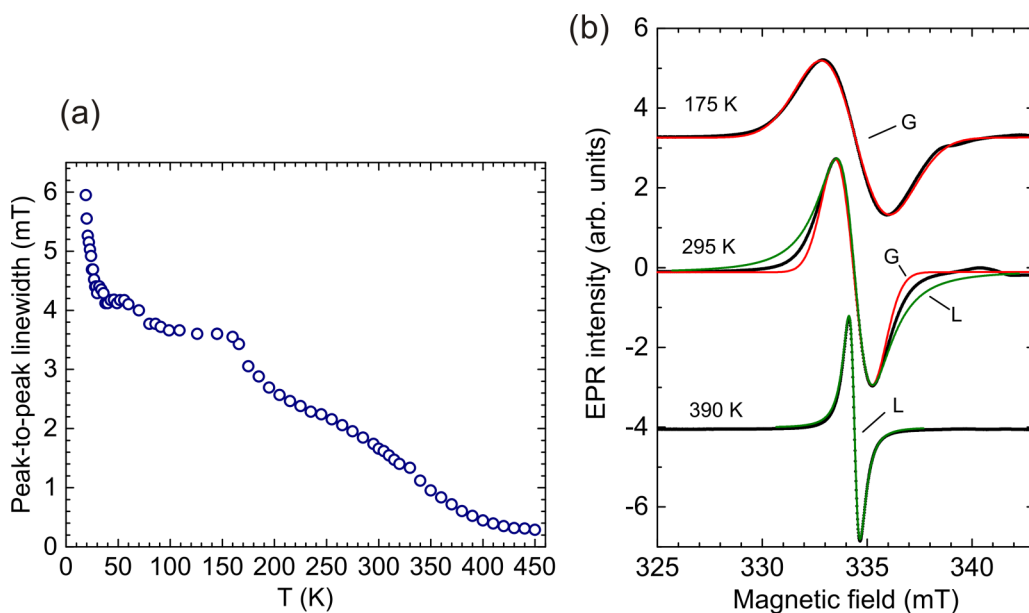


FIG. 7. (a) Temperature dependence of the peak-to-peak linewidth for the F^+ center in YAG at 9.4 GHz; (b) simulation of line shape at different temperatures: black points are experimental data; green and red solid lines are the Lorentzian and Gaussian fits, respectively.

One can see two temperature regions where the line becomes substantially narrower. In the first temperature region, it sharply decreases from ~ 6 to ~ 3.5 mT as the temperature increases from 20 to 100 K. The g factor at $T = 100$ K is $g_0 = \frac{1}{3}(g_1 + g_2 + g_3) = 1.994$. The narrowing of the spectrum can be explained in the following way: At the lowest temperature, where the F^+ center shows g factor anisotropy, the electron is well localized in the oxygen vacancy. When the temperature increases, the electron can thermally jump to another neighboring oxygen vacancy, not filled by an electron ($V_{O1}^\bullet + V_{O2} \rightarrow V_{O1} + V_{O2}^\bullet$ process), or there could be rather thermally assisted electron tunneling between oxygen vacancies. We cannot also exclude the situation of electron motion (exchange) between F^+ and F centers ($V_{O1}^{\bullet\bullet} + V_{O2}^\bullet \rightarrow V_{O1}^\bullet + V_{O2}^{\bullet\bullet}$ process) that will lead to averaging of the g factor anisotropy as well. Of course, such electron motion is possible when the distance between oxygen vacancies is not too large and does not exceed a few lattice constants at most, or when the electron wave function is quite delocalized. The motion mechanism will decrease the linewidth according to the following well-known relation [35]:

$$\Delta B_M = \gamma_e (\delta B_0)^2 \tau, \quad (4)$$

where δB_0 is half of the expected splitting in the spectrum due to g factor anisotropy (when the motion is frozen), γ_e is the electron gyromagnetic ratio, and τ is the relaxation time for charge hopping. This expression is valid at the condition $\gamma_e (\delta B_0) \tau \ll 1$, i.e., at the fast motion regime. For the thermally activated process, the relaxation time τ may be expressed in the form of the Arrhenius law:

$$\tau = \tau_0 \exp\left(\frac{E_a}{kT}\right), \quad (5)$$

where τ_0 is the high-temperature relaxation time and E_a is the activation energy. For the thermally assisted tunneling mechanism the expression for τ is more complex, but it

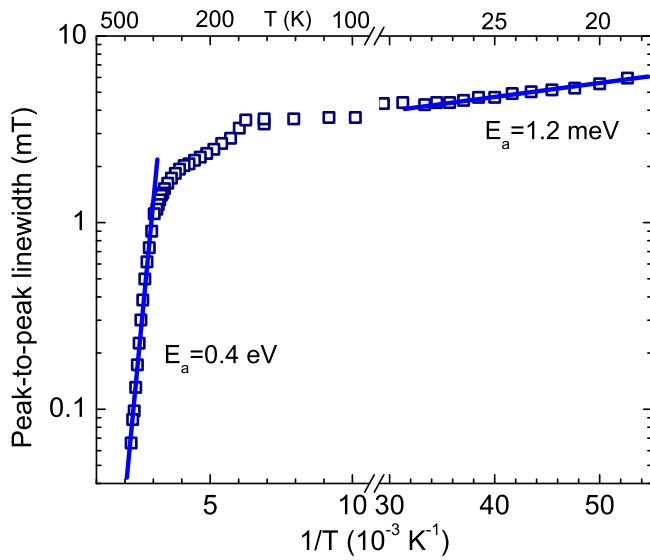


FIG. 8. Logarithmic plot of the peak-to-peak linewidth for the F^+ center as a function of the reciprocal temperature.

contains the exponential factor, too (see, e.g., [42]). The fit of the experimental linewidths at $T < 100$ K is shown in Fig. 8. Parameters of the fit are $E_a = 1.2$ meV and $\tau_0 \approx 5 \times 10^{-16}$ s. Such low activation energy suggests the tunneling mechanism as the thermal depth of the F^+ center should be much bigger. Note that our finding is supported by observation of background emission in thermally stimulated luminescence (TSL) of YAG/LuAG:Ce crystals at low temperatures, which only slightly depends on temperature. To explain this fact, a tunneling (or thermally assisted tunneling) of electrons to Ce ions in the garnet lattice was proposed [10]. The concentration of F^+ centers as determined from EPR intensity is about 5×10^{18} spins/cm³. It was measured by the spin counting method [43] using the reference MgO:Cr sample with known Cr³⁺ concentration. This concentration is comparable with the usual Ce concentration as a dopant.

The linewidth is almost constant between 100 and 180 K with the Gaussian shape. It is well described by taking into account Fermi contact HF interaction of electron spin with nuclear spins of two neighboring Al ions with the HF constants determined from ENDOR measurements, $A_1 = 10.7$ MHz and $A_2 = 13.2$ MHz. Each of the Al HF components is additionally broadened by a weak HF interaction with two neighboring ⁸⁹Y nuclei and more distant ²⁷Al nuclei. The simulated spectrum for $T = 175$ K is shown in Fig. 7(b), red line, as an example. Note that in our case, the motional narrowed line shape is Gaussian because it is determined by unresolved HF Fermi contact interaction of electron spin with surrounding nuclear spins.

It is completely surprising that the F^+ EPR spectrum continues to narrow with further temperature increase above ~ 200 K even though both the g factor and HF interaction are isotropic at these temperatures and the linewidth cannot be smaller than that determined by HF interaction. Moreover, the spectral line of a trapped electron usually broadens at such high temperatures due to increase of the spin-lattice relaxation rate. The narrowing of the F^+ spectral line indicates that

the Fermi contact interaction of the F^+ -center electron with neighboring nuclei reduces in value with temperature increase. The Fermi contact interaction is directly proportional to electron density at the nucleus,

$$A = \frac{8}{3} \beta \beta_N g g_N |\psi(0)|^2, \quad (6)$$

where β and β_N are the Bohr and nuclear magnetons, respectively; g_N is the nuclear g factor; and $\psi(0)$ is the electronic wave function at the nucleus. Therefore, according to the relation (6) substantial delocalization of the F^+ -center electron exists at $T > \sim 250$ K; i.e., at these temperatures the F^+ electron becomes a free electron in the conduction band, as for a donor electron in the n -type semiconductors [44]. The linewidth at $T > 250$ K follows exponential dependence on the reciprocal temperature with the activation energy ≈ 0.4 eV (Fig. 8). This energy can be considered as a very rough approximation of the electron binding energy. From this point of view, the F^+ center in YAG can be associated with a donor center as its temperature behavior is very similar to the behavior of a donor center in a semiconductor [44].

The increased radius of the wave function (delocalization) will also lead to exchange interaction between electron spins. The fast spin exchange with the exchange frequency ω_{ex} decreases the EPR spectrum width and leads to the so-called exchange narrowed line with the Lorentzian shape and width [45]:

$$\Delta B_{\text{ex}} = \gamma_e (\delta B_0)^2 / \omega_{\text{ex}}. \quad (7)$$

Allowing temperature dependence of the exchange frequency (determined by the exchange integral and thus the wave functions), one can obtain an additional source for spectrum narrowing.

The conduction band electrons can cause conductivity in the crystal. However, no direct current (dc) conductivity was detected in the YAG crystals with F^+ centers. Instead, the crystals show marked alternating current (ac) conductivity, which exponentially depends on the reciprocal temperature (Fig. 9). This suggests that conduction electrons do not travel across whole crystal due to inhomogeneities in crystal, when more conductive regions are separated by poorly conducting layers. For instance, the poorly conducting layers could be located near dislocations.

To check such a possibility, we measured the frequency dependence of the crystal capacitance recalculated in terms of dielectric constant. It shows typical behavior (Fig. 10) as for a dielectric material which contains highly conductive regions isolated (or separated) by low-conductive thin dielectric layers, so-called Maxwell-Wagner dielectric relaxation [46,47]. It predicts the following dispersion for the real part of dielectric constant of inhomogeneous semiconductor or dielectric [48]:

$$\varepsilon' = \varepsilon_\infty + \frac{\varepsilon_0^p - \varepsilon_1}{1 + \tau_\varepsilon^2 \omega^2}, \quad (8a)$$

$$\varepsilon_0^p = \varepsilon_2 \frac{x \rho_1^2 + \rho_2^2}{(x \rho_1 + \rho_2)^2}, \quad (8b)$$

$$\tau_\varepsilon = \varepsilon_0 \varepsilon_2 \frac{\rho_1 \rho_2}{x \rho_1 + \rho_2}, \quad (8c)$$

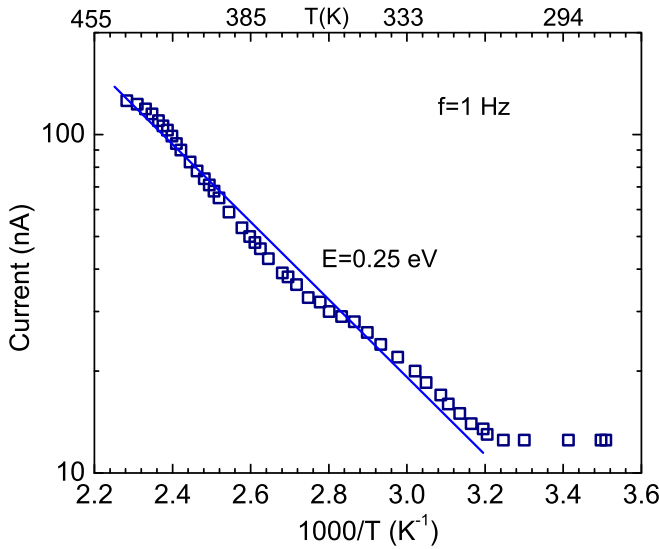


FIG. 9. Logarithmic plot of the ac current at applied ac field of 20 V/cm at the frequency 1 Hz as a function of the reciprocal temperature.

where ρ_1 , ρ_2 , and ε_1 , ε_2 denote the resistivity and the dielectric constant of the high-resistivity layers and the low-resistivity regions, respectively; $\varepsilon_0 = 8.85 \times 10^{-12} \text{ F m}^{-1}$, and $\omega = 2\pi f$ is the ac field frequency. It is also assumed that the ratio of the thickness of the high-resistivity layers to the thickness of low-resistivity regions is $x \ll 1$, and that $\varepsilon_1 = \varepsilon_2$, and $\rho_1 \gg \rho_2$.

Taking the dielectric permittivity of YAG $\varepsilon_2 = 11.7$, the calculated curve from Eqs. (8a)–(8c) follows well all characteristic features of the dielectric constant with frequency change (solid line in Fig. 10): the dielectric constant sharply increases at $f < 10^6$ Hz and approaches the dielectric permittivity of YAG $\varepsilon_2 = 11.7$ at $f > 10^7$ Hz. The following

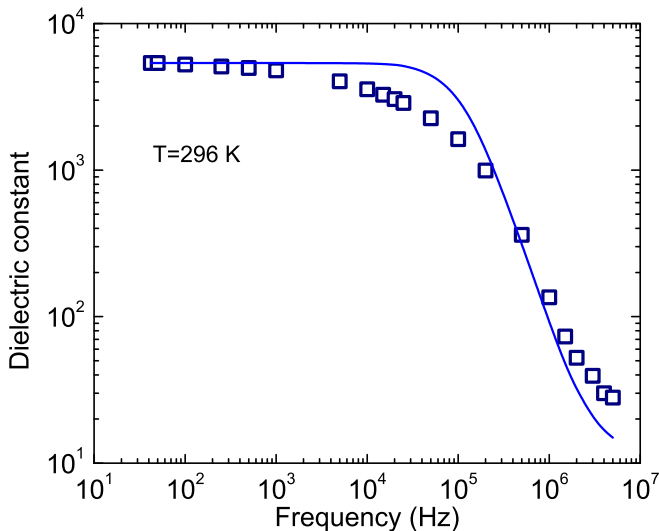


FIG. 10. Frequency dependence of the apparent dielectric constant at $T = 295$ K.

parameters were determined from the fit: $\varepsilon_0^p = 5370$, and $\tau_\varepsilon = 1.3 \times 10^{-6} \text{ s}^{-1}$. Unfortunately, Eqs. (8a)–(8c) do not allow determination of the ρ_1 , ρ_2 , and x parameters separately as the $x\rho_1$ can be comparable with ρ_2 value. Therefore, more experimental data are needed for determination of all parameters of the model, but this is beyond the scope of this paper.

Let us estimate the electron activation energy from the ac current measurements. Considering the low-temperature limit $E_a/kT \gg 1$, the conduction band electron concentration will vary with temperature as $\exp(-E_a/2kT)$. Then, neglecting the temperature dependence of electron mobility, we can take the same functional dependence for current as for the conduction band electron concentration. This gives $E_a = 0.5$ eV, the approximate depth of the F^+ -center donor level. It favorably agrees with the value ≈ 0.4 eV determined from the EPR measurements. The lifetime of the electron at oxygen vacancy according to Eq. (4) is $\sim 10^{-8}$ s at room temperature. This value agrees well with the 3.1 ns decay time of F^+ -center luminescence measured in a LuAG single crystal at room temperature [49].

IV. DISCUSSION AND CONCLUDING REMARKS

The energy $E_a = 0.4$ – 0.5 eV for an F^+ electron in YAG is considerably smaller as compared with that in simple oxides MgO and CaO [15], ZnO [50,51], and Al_2O_3 [41]). For instance, it was reported that the F^+ center in Al_2O_3 is thermally stable to the annealing temperature of 700 K [41]. Another fact to which we want to pay attention is that in complex oxides with two types of cation ions, as a rule, oxygen vacancy serves only as a perturbation for electron localization at one of the neighboring cation ions. In such a case, the oxygen vacancy is most probably filled by two electrons being a charge neutral defect. Such oxygen-vacancy center can be usually created in oxygen deficient crystals only by UV or x-ray irradiation at cryogenic temperature (at or below 77 K) since it is shallow. Its temperature stability is below room temperature. These centers are characterized by g factors of the cation ion, substantially shifted from the g factor of the free electron. For instance, the $\text{Pb}^+-\text{V}_\text{O}$ center in PbWO_4 has g factors between 1.22 and 1.61 [52]. Other examples are BaTiO_3 [53], PbTiO_3 [54], CaWO_4 [55], and Y_2SiO_5 [18]. The mechanism of electron localization for such oxygen-vacancy center is mainly related to the polaronic effect. The center can be thus considered as a small polaron bound to vacancy. From this point of view, the F^+ center in YAG is an example of the oxygen-vacancy center in complex oxides where an electron is located predominantly in oxygen vacancy and only weakly participates in covalent bonding with surrounding cations.

Finally, in conclusion we note that the results presented here for the F^+ center in YAG are not specific for our crystals only. A similar EPR spectral line from the F^+ center was measured in a YAG crystal reduced at 1500–1650 K [21], a colored YAG doped by Si [22], YAG crystals either γ irradiated or photoirradiated by UV nitrogen laser [20], and in additionally colored crystals [19]. However, no detailed studies of the F^+ -center behavior with temperature were performed in these early publications.

ACKNOWLEDGMENTS

The authors gratefully acknowledge the financial support of the Czech Science Foundation (Project No. 17-09933S), and the Ministry of Education, Youth and Sports of Czech Republic under Projects No. LO1409 and CZ.02.1.01/0.0/0.0/16_013/0001406. O.L. is grateful to the Baden-Württemberg Stiftung for the financial support by the Eliteprogramme for Postdocs. M.G.B. acknowledges the support from the National Recruitment Program of High-end Foreign Experts (Grants No. GDT20185200479 and No. GDW20145200225), Programme for the Foreign Experts (Grant No. W2017011) and Wenfeng High-end Tal-

ents Project (Grant No. W2016-01) offered by Chongqing University of Posts and Telecommunications (CQUPT), Estonian Research Council Grant No. PUT PRG111, European Regional Development Fund (TK141), and NCN Project No. 2018/31/B/ST4/00924. Partial support of the bilateral mobility project “Scintillation mechanisms in garnet- and perovskite-type crystals fabricated under different conditions” between Academies of Sciences of Ukraine and Czech Republic, and of Operational Programme Research, Development and Education financed by European Structural and Investment Funds and the Czech Ministry of Education, Youth and Sports (Project No. SOLID21 CZ.02.1.01/0.0/0.0/16_019/0000760) is also acknowledged with thanks.

- [1] W. Koechner, *Solid-State Laser Engineering*, 3rd ed. (Springer-Verlag, Berlin, 2006).
- [2] V. Lupei and A. Lupei, Nd:YAG at its 50th anniversary: Still to learn, *J. Lumin.* **169**, 426 (2016).
- [3] D. Y. Shen, J. K. Sahu, and W. A. Clarkson, Highly efficient in-band pumped Er:YAG laser with 60 W of output at 1645 nm, *Opt. Lett.* **31**, 754 (2006).
- [4] P. Lacovara, H. K. Choi, C. A. Wang, R. L. Aggarwal, and T. Y. Fan, Room-temperature diode-pumped Yb:YAG laser, *Opt. Lett.* **16**, 1089 (1991).
- [5] R. Atrata, P. Schauert, J. Kvapil, and J. Kvapil, A single crystal of YAG-new fast scintillator in SEM, *J. Phys. E: Sci. Instrum.* **11**, 707 (1978).
- [6] M. Nikl, V. V. Laguta, and A. Vedda, Complex oxide scintillators: Material defects and scintillation performance, *Phys. Status Solidi B* **245**, 1701 (2008).
- [7] O. Sidletskiy, K. Lebbou, D. Kofanov, V. Kononets, Ia Gerasymov, R. Bouaita, V. Jary, R. Kucerkova, M. Nikl, A. Polesel, K. Pauwels, and E. Auffray, Progress in fabrication of long transparent YAG: Ce and YAG: Ce, Mg single crystalline fibers for HEP applications, *Cryst. Eng. Commun.* **21**, 1728 (2019).
- [8] Z. Xia and A. Meijerink, Ce³⁺-doped garnet phosphors: Composition modification, luminescence properties and applications, *Chem. Soc. Rev.* **46**, 275 (2017).
- [9] W. Chewpraditkul, L. Swiderski, M. Moszynski, T. Szczesniak, A. Syntfeld-Kazuch, C. Wanarak, and P. Limsuwan, Scintillation properties of LuAG:Ce, YAG:Ce and LYSO:Ce crystals for gamma-ray detection, *IEEE Trans. Nucl. Sci.* **56**, 3800 (2009).
- [10] M. Nikl, A. Vedda, M. Fasoli, I. Fontana, V. V. Laguta, E. Mihokova, J. Pejchal, J. Rosa, and K. Nejezchleb, Shallow traps and radiative recombination processes in Lu₃Al₅O₁₂:Ce single crystal scintillator, *Phys. Rev. B* **76**, 195121 (2007).
- [11] M. M. Kuklja, Defects in yttrium aluminium perovskite and garnet crystals: Atomistic study, *J. Phys.: Condens. Matter* **12**, 2953 (2000).
- [12] M. Nikl, E. Mihokova, J. Pejchal, A. Vedda, Y. Zorenko, and K. Nejezchleb, The antisite Lu_{Al} defect and related trap in Lu₃Al₅O₁₂:Ce single crystal, *Phys. Status Solidi B* **242**, R119 (2005).
- [13] C. R. Stanek, K. J. McClellan, M. R. Levy, C. Milanese, and R. W. Grimes, The effect of intrinsic defects on RE₃Al₅O₁₂ garnet scintillator performance, *Nucl. Instrum. Methods. Phys. Res., Sect. A* **579**, 27 (2007).
- [14] V. V. Laguta, M. Nikl, A. Vedda, E. Mihokova, J. Rosa, and K. Blazek, Hole and electron traps in the YAlO₃ single crystal scintillator, *Phys. Rev. B* **80**, 045114 (2009).
- [15] B. Henderson and J. E. Wertz, Defects in the alkaline earth oxides, *Adv. Phys.* **17**, 749 (1968).
- [16] K. O'Donnell, R. C. Barklie, and B. Henderson, EPR and optical absorption studies of radiation-produced defects in sodium P-alumina, *J. Phys. C: Solid State Phys.* **11**, 3871 (1978).
- [17] S. V. La, R. H. Bartram, and R. T. Cox, The F⁺ centers in reactor-irradiated aluminum oxide, *J. Phys. Chem. Solids* **34**, 1079 (1973).
- [18] V. V. Laguta, M. Buryi, J. Rosa, D. Savchenko, J. Hybler, M. Nikl, S. Zazubovich, T. Kärner, C. R. Stanek, and K. J. McClellan, Electron and hole traps in yttrium orthosilicate single crystals: The critical role of Si-unbound oxygen, *Phys. Rev. B* **90**, 064104 (2014).
- [19] K. Mori, Transient colour centers caused by UV light irradiation in yttrium aluminium garnet crystals, *Phys. Status Solidi A* **42**, 375 (1977).
- [20] L. G. Karaseva, N. Yu. Konstantinov, and V. V. Gromov, Nature of radiation colour centers in single crystals of yttrium aluminum garnet, *Radiat. Phys. Chem.* **26**, 723 (1985).
- [21] C. Y. Chen, G. J. Pogatschnik, Y. Chen, and M. R. Kokta, Optical and electron paramagnetic resonance studies of Fe impurities in yttrium aluminum garnet crystals, *Phys. Rev. B* **38**, 8555 (1988).
- [22] D. Fagundes-Peters, N. Martynyuk, K. Lunstedt, V. Peters, K. Petermann, G. Huber, S. Basun, V. V. Laguta, and A. Hofstaetter, High quantum efficiency of YbAG-crystals, *J. Lumin.* **125**, 238 (2007).
- [23] V. Laguta, M. Buryi, J. Pejchal, V. Babin, and M. Nikl, Hole Self-Trapping in Y₃Al₅O₁₂ and Lu₃Al₅O₁₂ Garnet Crystals, *Phys. Rev. Appl.* **10**, 034058 (2018).
- [24] M. Springis, A. Pujats, and J. Valbis, Polarization of luminescence of colour centers in YAG crystals, *J. Phys.: Condens. Matter* **3**, 5457 (1991).
- [25] A. Pujas and M. Springis, The F-type centers in YAG crystals, *Radiat. Eff. Defects Solids* **155**, 65 (2001).
- [26] E. Mihoková, M. Nikl, J. A. Mareš, A. Beitlerová, A. Vedda, K. Nejezchleb, K. Blažek, and C. D'Ambrosio, Luminescence

- and scintillation properties of YAG:Ce single crystal and optical ceramics, *J. Lumin.* **126**, 77 (2007).
- [27] Y. Zorenko, V. Gorbenko, I. Konstankevych, A. Voloshinovskii, G. Stryganyuk, V. Mikhailin, V. Kolobanov, and D. Spassky, Single-crystalline films of Ce-doped YAG and LuAG phosphors: Advantages over bulk crystals analogues, *J. Lumin.* **114**, 85 (2005).
- [28] A. Ponti and A. Schweiger, Echo phenomena in electron paramagnetic resonance spectroscopy, *Appl. Magn. Reson.* **7**, 363 (1994).
- [29] P. Arhipov, S. Tkachenko, S. Vasiukov, K. Hubenko, Ia. Gerasymov, V. Baumer, A. Puzan, P. Mateychenko, K. Lebbou, and O. Sidletskiy, Features of YAG growth under Ar+Co reducing atmosphere, *J. Cryst. Growth* **449**, 104 (2016).
- [30] S. Tkachenko, P. Arhipov, I. Gerasymov, D. Kurtsev, S. Vasyukov, V. Nesterkina, N. Shiran, P. Mateichenko, and O. Sidletskiy, Control of optical properties of YAG crystals by thermal annealing, *J. Cryst. Growth* **483**, 195 (2018).
- [31] W. B. Mims, Pulsed ENDOR experiment, *Proc. R. Soc.* **283**, 452 (1965).
- [32] E. R. A. Davies, A new pulsed ENDOR technique, *Phys. Lett. A* **47**, 1 (1974).
- [33] P. Neugebauer, D. Bloos, R. Marx, P. Lutz, M. Kern, D. Aguila, J. Vaverka, O. Laguta, C. Dietrich, R. Clerac, and J. van Slageren, Ultra-broadband EPR spectroscopy in field and frequency domains, *Phys. Chem. Chem. Phys.* **20**, 15528 (2018).
- [34] S. Geschwind, Paramagnetic resonance of Fe^{3+} in octahedral and tetrahedral sites in yttrium gallium garnet (YGaG) and anisotropy of yttrium iron garnet (YIG), *Phys. Rev.* **121**, 363 (1961).
- [35] A. Abragam, *Principles of Nuclear Magnetism* (Oxford University Press, New York, 1961).
- [36] I. Laulicht, Y. Yacobi, and A. Baram, The charge state of Mn and defect dynamics in manganese doped $\text{KTa}_x\text{Nb}_{1-x}\text{O}_3$, *J. Chem. Phys.* **91**, 79 (1989).
- [37] F. Euler and J. A. Bruce, Oxygen coordinates of compounds with garnet structure, *Acta Crystallogr.* **19**, 971 (1965).
- [38] Th. Vosegaard, I. P. Byriel, D. A. Pawlak, K. Wozniak, and H. J. Jakobsen, Crystal structure studies on the garnet $\text{Y}_3\text{Al}_5\text{O}_{12}$ by ^{27}Al single-crystal NMR spectroscopy, *J. Am. Chem. Soc.* **120**, 7900 (1998).
- [39] V. Laguta, Yu. Zorenko, V. Gorbenko, A. Iskalyeva, Yu. Zagorodniy, O. Sidletskiy, P. Bilski, A. Twardak, and M. Nikl, Aluminium and gallium substitution in solid solutions of yttrium aluminium-gallium garnets single crystals: Investigation by NMR method, *J. Phys. Chem. C* **120**, 24400 (2016).
- [40] L. Kevan and L. D. Kispert, *Electron Spin Double Resonance Spectroscopy* (John Wiley and Sons, New York, 1979).
- [41] R. Ramirez, M. Tardio, R. Gonzalez, and J. E. Munoz Santiuste, Optical properties of vacancies in thermochemically reduced Mg-doped sapphire single crystals, *J. Appl. Phys.* **101**, 123520 (2007).
- [42] J. A. Sussmann, Quantum mechanical theory of barrier crossing by ions in solids, *J. Phys. Chem. Solids* **28**, 1643 (1967).
- [43] S. K. S. Parashar, B. S. Murty, S. Repp, S. Weber, and E. Erdem, Investigation of intrinsic defects in core-shell structured ZnO nanocrystals, *J. Appl. Phys.* **111**, 113712 (2012).
- [44] G. W. Ludwig and H. H. Woodbury, Electron spin resonance in semiconductors, *Solid State Phys.* **13**, 223 (1962).
- [45] P. W. Anderson and P. R. Weiss, Exchange narrowing in paramagnetic resonance, *Rev. Mod. Phys.* **25**, 269 (1953).
- [46] J. C. Maxwell, *Electricity and Magnetism* (Oxford University Press, London, 1873), Vol. I, Sec. 328.
- [47] K. W. Wagner, Erklärung der dielektrischen nachwirkungsvorgänge auf grund Maxwellscher vorstellungen, *Arch. Electrotech.* **2**, 371 (1914).
- [48] C. G. Koops, On the dispersion of resistivity and dielectric constant of some semiconductors at audiofrequencies, *Phys. Rev.* **83**, 121 (1951).
- [49] V. Babin, V. V. Laguta, A. Maaros, A. Makhov, M. Nikl, and S. Zazubovich, Luminescence of F^{+} -type centers in undoped $\text{Lu}_3\text{Al}_5\text{O}_{12}$ single crystals, *Phys. Status Solidi B* **248**, 239 (2011).
- [50] J. M. Smith and W. E. Vehse, ESR of electron irradiated ZnO confirmation of the F^{+} center, *Phys. Lett. A* **31**, 147 (1970).
- [51] L. S. Vlasenko, Magnetic resonance studies of intrinsic defects in ZnO: Oxygen vacancies, *Appl. Magn. Reson.* **39**, 103 (2010).
- [52] V. V. Laguta, M. Martini, A. Vedda, M. Nikl, E. Mihóková, P. Boháček, J. Rosa, A. Hofstätter, B. K. Meyer, and Y. Usuki, Photoinduced Pb^{+} center in PbWO_4 : Electron spin resonance and thermally stimulated luminescence study, *Phys. Rev. B* **64**, 165102 (2001).
- [53] S. Lenjer, O. F. Schirmer, H. Hesse, and Th. W. Kool, Conduction states in oxide perovskites: Three manifestations of Ti^{3+} Jahn-Teller polarons in barium titanate, *Phys. Rev. B* **66**, 165106 (2002).
- [54] V. V. Laguta, M. D. Glinchuk, I. P. Bykov, Yu. L. Maksimenko, J. Rosa, and L. Jastrabík, Impurity centers in PbTiO_3 single crystals: An electron-spin-resonance analysis, *Phys. Rev. B* **54**, 12353 (1996).
- [55] K. C. Chu and C. Kikuchi, Direct measurements of the oxygen vacancies produced in calcium tungstate by fast reactor neutrons, *Phys. Rev.* **169**, 752 (1968).